

Observational Constraints on Two-field Warm Inflation

Yang-yang Wang* and Jian-Yang Zhu†

Department of Physics, Beijing Normal University, Beijing 100875, China

Xiao-Min Zhang‡

School of Science, Qingdao University of Technology, Qingdao 266033, China

We study the two-field warm inflation models with a double quadratic potential and a linear temperature dependent dissipative coefficient. We derived the evolution equation of all kinds of perturbations without assuming slow-roll approximation, and obtained the curvature power spectrum at the end of inflation with a fully numerical method. Then we compute the scalar spectral index n_s , tensor-to-scalar ratio r for several representative potentials, and compare our results with observational data. At last, we use Planck data to constrain the parameters in our models. This work is a natural extension of single-field warm inflation, and the aim of this work is to present some features of multi-field warm inflation using a simple two-field model.

PACS numbers: 98.80.Cq

I. INTRODUCTION

Inflation is widely accepted as the leading theory describing the early Universe [1–3], because it solves many long-standing puzzles of the hot big bang model, such as the horizon, flatness, and monopole problems. In addition, primordial fluctuations generated in inflation provide the seed for the large-scale structure of our Universe, and it can explain the temperature anisotropies on cosmic microwave background (CMB) naturally. In standard cold inflation, cosmological expansion and reheating are two separate period and we still know little about the details of reheating. The recent observational results have reached an impressive level of precision and improved the upper bound on tensor-to-scalar ratio r , so many representative models are ruled out in standard inflationary paradigm.

Warm inflation is an alternative to standard cold inflation [4], where the interaction between inflaton and radiation can cause an extra dissipative term. The dissipative effects can lead to a sustainable radiation production, so the Universe can become radiation-dominated without reheating process. In warm inflation, density fluctuations come from thermal fluctuation, which is much larger than quantum fluctuations in cold inflation. Consequently, warm inflation can happen at a much smaller energy scale, and this leads to suppressed tensor-to-scalar ratio. Many inflationary potentials excluded in cold inflation become consistent with observations again in warm inflation. There have been various studies on warm inflation [5–8], and many interesting features are explored. Although warm inflation remains an appealing alternative to standard cold inflation, realizing warm inflation in concrete models is not easy. When coupling the inflaton

directly with light fields, we have to make sure that the thermal corrections to the inflaton potential is not large, so that the inflaton potential remains flat and we can get sufficient e-foldings. At the same time, the dissipative effects should be strong enough to sustain a thermal bath at temperature $T > H$ during inflationary universe. In Ref. [9], the authors examined the feasibility of warm inflation from various viewpoint, and showed that it was extremely difficult or perhaps even impossible to realize the idea of warm inflation. Recently, a scenario fulfilling these conditions has been proposed in [10], where the inflaton is a pseudo-Goldstone-boson coupled to a pair of fermionic fields through Yukawa interactions. In this case, the inflaton's mass gets protection from large thermal corrections due to the symmetries obeyed by the model, so the slow-roll of warm inflation will not be affected. This leads to enough dissipation with only a small number of fields, and a linear T dissipative coefficient.

The simplest inflationary models comprise only a single scalar degree of freedom, which are sufficient to obtain predictions consistent with observational constraints. Single-field inflation may seem natural from the perspective of simplicity and economy, but the status is not certain from perspective of microphysical origin of inflation [11]. In fact, fundamental physics seems to predict the existence of a large number of scalar fields [12]. If the inflationary scale is not widely separated from the next relevant mass scale, it is natural to expect inflationary models with more than one active scalar fields. Inflation driven by multiple scalar fields has some specific features, such as large non-Gaussianity [13–15], the presence of isocurvature perturbation [16, 17], which can be narrowly constrained by the improved observational data in the future.

The content of the early universe is usually treated as a mixture of radiation fluid and scalar fields, in which interactions between different fields and dissipative effects play an important role. Therefore, to study the dynamical and perturbation features of multi-component cosmology and how it is constrained by observation is an

*Electronic address: wangyy@mail.bnu.edu.cn

†Corresponding author; Electronic address: zhuji@bnu.edu.cn

‡Electronic address: zhangxm@mail.bnu.edu.cn

important topic. One of the models including all these effects is the multi-field warm inflation paradigm, in which the radiation is regarded as a perfect fluid. In this paper we will focus on two-field warm inflation and try to reveal some features of multi-field inflation by constraining our models with observation data. In our previous work [18], we have shown some simple conclusions in a temperature(T) independent dissipative coefficient γ , which is not a realistic case. Now we extend our analysis as a next step to a linear T dissipative coefficient. In Ref. [10] it has been shown that a dissipative coefficient $\gamma = C_T T$ can be realized in a Little Higgs model, which put warm inflation on a solid footing in the aspect of model building.

This work is organized as follows. In Section II, we introduce some basics of two-field warm inflation, and derive the full set of equations describing the background dynamics and perturbations. In Section III, we give the main features of two-field warm inflation by numerically solving the equations obtained in Section II. In Section IV, we use the Planck data to constrain our models, and give the observational constraints on model parameters. In Section IV, we present our conclusions.

II. BASICS OF TWO-FIELD WARM INFLATION

The two-field warm inflation dynamics is characterized by the coupled background equations of inflaton field $\phi(t)$, $\chi(t)$ and radiation density $\rho_r(t)$,

$$\begin{aligned} \ddot{\phi} + (3H + \gamma)\dot{\phi} + V_\phi &= 0, \\ \ddot{\chi} + (3H + \gamma)\dot{\chi} + V_\chi &= 0, \\ \dot{\rho}_r + 4H\rho_r &= \gamma(\dot{\phi}^2 + \dot{\chi}^2), \end{aligned} \quad (2.1)$$

where V is the inflaton potential, $V_\phi = \partial V(\phi, \chi)/\partial\phi$, $V_\chi = \partial V(\phi, \chi)/\partial\chi$, overdots represent derivatives with respect to cosmic time t , and γ is dissipative coefficient. In general case, γ is a function of background inflaton fields and the temperature T . For simplicity, we will use the Planck Unit in the following context,

$$8\pi G = k_B = \hbar = c = 1,$$

where G is Newton's gravitational constant, k_B is Boltzmann's constant, \hbar is the reduced Planck's constant, and c is the speed of light. In a spatially flat universe, the Friedmann equations read:

$$3H^2 = \frac{1}{2}\dot{\phi}^2 + \frac{1}{2}\dot{\chi}^2 + V(\phi, \chi) + \rho_r, \quad (2.2)$$

and the slow-roll parameters are defined as,

$$\epsilon = -\frac{\dot{H}}{H^2}, \quad \eta = -\frac{\ddot{H}}{2H\dot{H}}. \quad (2.3)$$

Inflation takes place when the slow-roll condition $\epsilon < 1$, $|\eta| < 1$ are satisfied. In slow-roll approximation we have,

$$(3H + \gamma)\dot{\phi} + V_\phi = 0, \quad (2.4)$$

$$(3H + \gamma)\dot{\chi} + V_\chi = 0, \quad (2.5)$$

$$4H\rho_r = \gamma(\dot{\phi}^2 + \dot{\chi}^2). \quad (2.6)$$

For convenience, we define adiabatic field σ and entropy field s by making a rotation in field space, where $d\sigma$ is tangent to the background trajectory and ds is normal to it [19, 20],

$$\begin{pmatrix} d\sigma \\ ds \end{pmatrix} = \begin{pmatrix} \cos\theta & \sin\theta \\ -\sin\theta & \cos\theta \end{pmatrix} \begin{pmatrix} d\phi \\ d\chi \end{pmatrix}, \quad (2.7)$$

where $\cos\theta = \frac{\dot{\phi}}{\sqrt{\dot{\phi}^2 + \dot{\chi}^2}}$, $\sin\theta = \frac{\dot{\chi}}{\sqrt{\dot{\phi}^2 + \dot{\chi}^2}}$. With this definition, the background equations Eqs. (2.1) and (2.2) become,

$$\begin{aligned} \ddot{\sigma} + (3H + \gamma)\dot{\sigma} + V_\sigma &= 0, \\ \dot{\theta}\dot{\sigma} + V_s &= 0, \\ \dot{\rho}_r + 4H\rho_r &= \gamma\dot{\sigma}^2, \\ 3H^2 &= \frac{1}{2}\dot{\sigma}^2 + V + \rho_r \end{aligned} \quad (2.8)$$

where $V_\sigma = \cos\theta V_\phi + \sin\theta V_\chi$, $V_s = -\sin\theta V_\phi + \cos\theta V_\chi$. In this case, slow-roll parameters can be expressed by,

$$\begin{aligned} \epsilon &= \epsilon_\sigma + \epsilon_r, \quad \epsilon_\sigma = \frac{1}{2} \frac{\dot{\sigma}^2}{H^2}, \quad \epsilon_r = \frac{2}{3} \frac{\rho_r}{H^2}, \\ \eta &= \frac{\epsilon_\sigma}{\epsilon} \eta_\sigma + \frac{\epsilon_r}{\epsilon} \eta_r, \quad \eta_\sigma = -\frac{\ddot{\sigma}}{H\dot{\sigma}}, \quad \eta_r = -\frac{1}{2} \frac{\dot{\rho}_r}{H\rho_r}. \end{aligned} \quad (2.9)$$

In order to study the evolution of perturbations, we decompose each of the fields into a spatially homogeneous background field and its perturbations, $\phi(x, t) \rightarrow \phi(t) + \delta\phi(x, t)$, $\chi(x, t) \rightarrow \chi(t) + \delta\chi(x, t)$. Similarly, it is convenient to decompose the field perturbation into an adiabatic component $\delta\sigma$ and entropy component δs [21],

$$\begin{pmatrix} \delta\sigma \\ \delta s \end{pmatrix} = \begin{pmatrix} \cos\theta & \sin\theta \\ -\sin\theta & \cos\theta \end{pmatrix} \begin{pmatrix} \delta\phi \\ \delta\chi \end{pmatrix}. \quad (2.10)$$

The line element of the Friedmann-Robertson-Walker (FRW) metric is given by,

$$\begin{aligned} ds^2 &= -(1 + 2A)dt^2 + 2a\partial_i B dx^i dt \\ &+ a^2((1 - 2\psi)\delta_{ij} + 2\partial_i \partial_j E) dx^i dx^j. \end{aligned} \quad (2.11)$$

In warm inflation, we have to take into account the perturbations result from both the inflation field and radiation. Therefore, the total gauge-invariant comoving curvature perturbation can be split into two parts [22–24],

$$\mathcal{R} = \frac{\epsilon_\sigma}{\epsilon} \mathcal{R}_\sigma + \frac{\epsilon_r}{\epsilon} \mathcal{R}_r, \quad (2.12)$$

where $\mathcal{R}_\sigma = \psi + H \frac{\delta\sigma}{\sigma}$, $\mathcal{R}_r = \psi - aH(B + \delta u)$, and δu is the scalar velocity potential of the radiation fluid. For convenience, we also define the isocurvature perturbation $\mathcal{S} = H \frac{\delta s}{\sigma}$. The power spectrum of comoving curvature \mathcal{R} perturbation is given by,

$$\mathcal{P}_{\mathcal{R}} = \frac{k^3}{2\pi^2} \langle \mathcal{R}^2 \rangle, \quad (2.13)$$

and the power spectrum of inflaton perturbation \mathcal{R}_σ , radiation perturbation \mathcal{R}_r and isocurvature perturbation \mathcal{S} are [25],

$$\mathcal{P}_\sigma = \frac{k^3}{2\pi^2} \langle \mathcal{R}_\sigma^2 \rangle, \quad \mathcal{P}_r = \frac{k^3}{2\pi^2} \langle \mathcal{R}_r^2 \rangle, \quad \mathcal{P}_\mathcal{S} = \frac{k^3}{2\pi^2} \langle \mathcal{S}^2 \rangle, \quad (2.14)$$

where k denotes comoving wave number. In warm inflation, density perturbations mainly arise from thermal noise [26]. On small scales ($k \gg aH$) the metric fluctuations have little effects [27, 28], so inflaton fluctuations $\delta\varphi_I$ ($\delta\varphi_I = \delta\phi, \delta\chi$) are described by a Langevin equation [29],

$$\delta\ddot{\varphi}_I(k, t) + (3H + \gamma)\delta\dot{\varphi}_I(k, t) + \frac{k^2}{a^2}\delta\varphi_I = \xi_I(k, t), \quad (2.15)$$

where $\xi_I(k, t)$ is a white-noise term and different components of $\xi_I(k, t)$ is independent of each other. In this case, there is no coupling between different components of inflaton perturbations before horizon-crossing, which is a common assumption in standard multi-field inflation. In the high temperature limit, the noise source is Markovian,

$$\langle \xi_I(k, t)\xi_J(-k', t') \rangle = 2\gamma T a^{-3} (2\pi)^3 \delta_{IJ} \delta^3(k - k') \delta(t - t'), \quad (2.16)$$

where T denotes the temperature and a is the scales factor. The relationship between radiation energy density ρ_r and T is $\rho_r = \frac{\pi^2}{30} g_* T^4$, where g_* is the effective particle number of radiation fluid [30]. We will take $g_* = 228.75$ in the following numerical calculation, which is the number of degrees of freedom for the Minimal Supersymmetric Standard Model [31, 32]. After horizon-crossing, the effects of thermal noise are suppressed while the metric perturbation come to play an important role [33]. In previous studies, the perturbations in sub-horizon and super-horizon scales are often treated separately for simplicity. The power spectrum in warm inflation has been studied in many previous works [34–36], and a general expression for amplitude of inflaton power spectrum is given by [37],

$$\mathcal{P}_{\delta\sigma}^* = \left(\frac{H_*}{2\pi} \right)^2 \left(\frac{T_*}{H_*} \frac{2\pi Q_*}{\sqrt{1 + 4\pi Q_*/3}} + 1 + 2n_* \right) G(Q_*), \quad (2.17)$$

where a subscript “*” denotes variables evaluated at horizon crossing, $Q = \gamma/(3H)$ is the dissipative ratio, and $n_* = 1/(e^{H_*/T_*} - 1)$ is the statistical distribution of inflaton fluctuations at horizon crossing [38]. The function $G(Q_*)$ represents the growth of $\mathcal{P}_{\mathcal{R}}$ due to the coupling between inflaton fluctuations and radiation fluctuations, and this growing function can only be determined by solving the perturbation equations numerically.

When performing numerical calculations, it is more convenient to take e-foldings N ($dN = Hdt$) as the time variable. In order to get a full picture of the evolution of perturbations, we take into account all kinds of perturbations in two-field warm inflation, and give the evolution equation of \mathcal{R}_σ , \mathcal{R}_r and δs beyond slow-roll approximation (see Appendix A for more details),

$$\begin{aligned} \mathcal{R}_\sigma'' + (3 + 3Q + \epsilon_r + \epsilon_\sigma - 2\eta_\sigma) \mathcal{R}_\sigma' + (z^2 - 2\lambda_\theta^2 \epsilon_\sigma - 9Q + 2(1 + \epsilon_r - \eta_\sigma)\epsilon_r + Q(3\epsilon_r - 11\epsilon_\sigma + 6\eta_r)) \mathcal{R}_\sigma \\ = -(3Q + 2\epsilon_r) \mathcal{R}_r' + (-9Q + 2(1 + \epsilon_r - \eta_\sigma)\epsilon_r + Q(3\epsilon_r - 11\epsilon_\sigma + 6\eta_r)) \mathcal{R}_r \\ + 2\lambda_\theta \delta s' + 2(\lambda_\theta(3 + 3Q - \epsilon_r - \eta_\sigma) + \lambda_{\theta\theta}) \delta s + \frac{z^{3/2} k^{-3/2}}{\sqrt{2\epsilon_\sigma}} \xi_\sigma, \end{aligned} \quad (2.18)$$

$$\begin{aligned} \mathcal{R}_r'' + \left(6 + \epsilon_r + \epsilon_\sigma - \frac{7}{2}\eta_r \right) \mathcal{R}_r' \\ + \left(\frac{1}{3}z^2 + 9 + \frac{1}{2}(-9 + \epsilon_\sigma)\eta_r + 2(4 + \epsilon_\sigma - 2\eta_r)(\epsilon_r + \epsilon_\sigma - \eta_\sigma) + \left(-1 + Q + \frac{2}{3}\epsilon_r \right) \epsilon_\sigma \right) \mathcal{R}_r \\ = \left(\frac{2}{3}\epsilon_\sigma + \frac{5}{4}(4 - 2\eta_r) \right) \mathcal{R}_\sigma' + \left(9 + \frac{1}{2}(-9 + \epsilon_\sigma)\eta_r + 2(4 + \epsilon_\sigma - 2\eta_r)(\epsilon_r + \epsilon_\sigma - \eta_\sigma) + \left(-1 + Q + \frac{2}{3}\epsilon_r \right) \epsilon_\sigma \right) \mathcal{R}_\sigma \\ + \frac{1}{3}(-6 + 2\epsilon_\sigma + 3\eta_r)\lambda_\theta \delta s, \end{aligned} \quad (2.19)$$

$$\delta s'' + (3 + 3Q - \epsilon_r - \epsilon_\sigma)\delta s' + \left(z^2 + \frac{V_{ss}}{H^2} - 2\lambda_\theta^2\epsilon_\sigma\right)\delta s = -4\lambda_\theta\epsilon_\sigma\mathcal{R}_\sigma' - 4\lambda_\theta\epsilon_\sigma\epsilon_r\mathcal{R}_\sigma + 4\lambda_\theta\epsilon_\sigma\epsilon_r\mathcal{R}_r + z^{3/2}k^{-3/2}\xi_s, \quad (2.20)$$

where a prime denotes a derivative with respect to e-folding N , and $\lambda_\theta = \theta'/\sigma'$, $\lambda_{\theta\theta} = \theta''/\sigma'$. $V_{ss} = \sin^2\theta V_{\phi\phi} + \cos^2\theta V_{\chi\chi}$ is the effective mass of entropy field s , and $z = \frac{k}{aH}$. ξ_σ, ξ_s are two gaussian white noise and their correlation function are,

$$\langle \xi_I(k, N)\xi_J(-k', N') \rangle = 2\gamma T(2\pi)^3 \delta_{IJ}\delta^{(3)}(k-k')\delta(N-N') \quad (2.21)$$

where $I, J = \sigma, s$. Similarly, using N as the time variable, we can put Eqs. (2.1) and (2.2) in the form,

$$\phi'' + (3 + 3Q - \epsilon)\phi' + \frac{V_\phi}{H^2} = 0, \quad (2.22)$$

$$\chi'' + (3 + 3Q - \epsilon)\chi' + \frac{V_\chi}{H^2} = 0, \quad (2.23)$$

$$\rho_r' + 4\rho_r = 3H^2Q(\phi'^2 + \chi'^2), \quad (2.24)$$

$$\left(3 - \frac{1}{2}\phi'^2 - \frac{1}{2}\chi'^2\right)H^2 = V + \rho_r. \quad (2.25)$$

Note that the slow-roll parameters in above equations are treated as a function of time variable N , and can be determined by solving background equations Eqs. (2.22), (2.23), (2.24) and (2.25). When dealing with multi-field inflation, it is necessary to go beyond slow-roll, or we will miss some important features. In this case, the numerical method is almost essential, because we can hardly find any analytic results.

III. NUMERICAL EXAMPLES

In order to get a picture of the dynamics and perturbations of two-field warm inflation, we apply the formalism to a simple example in this section. We use the two-field quadratic inflation as an example, in which the potential is given by [39],

$$V(\phi, \chi) = \frac{1}{2}m_\phi^2\phi^2 + \frac{1}{2}m_\chi^2\chi^2. \quad (3.1)$$

Although these two scalar fields have no direct coupling, they can interact gravitationally during inflation. We will show that even the simplest two-field warm inflation models can display interesting features, which is very different from the single-field cases. In the following calculations, we set $N = 0$ when the relevant scales cross the Hubble horizon, and we fix $N_e = 60$ when inflation ends for definite calculation.

At the beginning of our analysis, we use a representative example to demonstrate the main features of background dynamics and perturbations of two-field warm

inflation. In the example, we set $m_\phi = 2 \times 10^{-8}$, and the

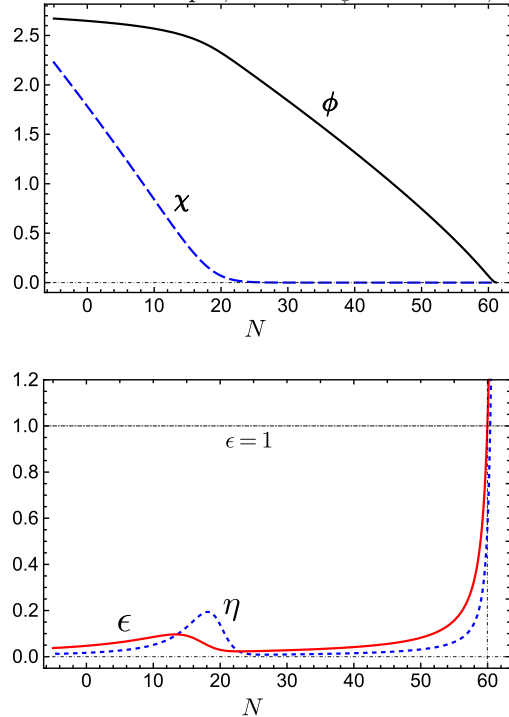


FIG. 1: The evolution of inflaton (ϕ, χ) and slow-roll parameters ϵ, η are shown against e-foldings N . In this example, we choose the initial condition $(\phi_0, \chi_0) = (2.67, 2.23)$, $C_T = 0.048$, and inflation ends at about $N = 60$ in this case. From the lower panel, we can know that when the field χ decay to zero, a local extreme occurs for slow-roll parameters ϵ and η .

mass ratio $R_m = m_\chi/m_\phi = 5$. After choosing the initial condition $(\phi_0, \chi_0) = (2.67, 2.23)$ and $C_T = 0.0483$, we can perform our numerical computation by solving the background equations Eqs. (2.22), (2.23), (2.24), (2.25) and stochastic perturbation equations Eqs. (2.18), (2.19) and (2.20). Note that since the background dynamics will tend to the slow-roll trajectory soon, the initial value of $\dot{\phi}_*, \dot{\chi}_*$ and ρ_{r*} have little impact on the final results. In order to eliminate the influence of initial conditions of perturbations equations, we begin our numerical integration about 5 e-foldings before Hubble exit. The results are shown in Fig. 1 and Fig. 2.

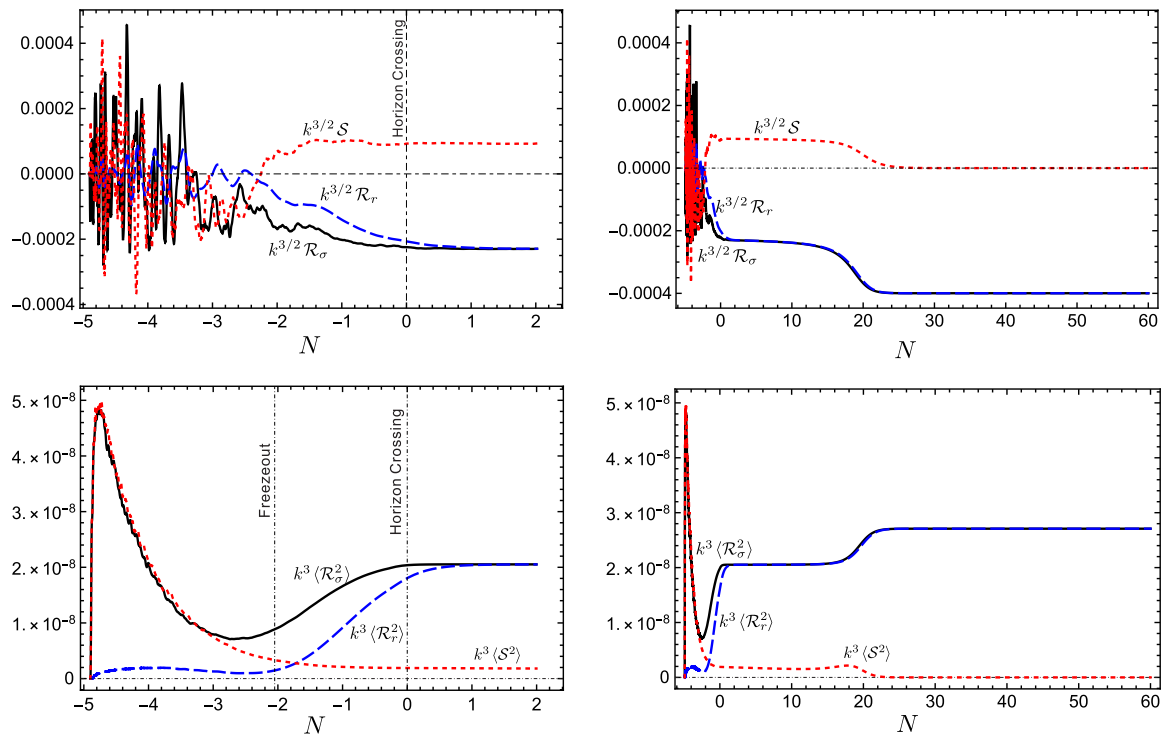


FIG. 2: The evolution of perturbations \mathcal{R}_σ , \mathcal{R}_r , \mathcal{S} , and the power spectrum of each kind of perturbations are shown in this figure. In the top two panels, we show a single realization of stochastic perturbation equation, and the power spectrum of each perturbation are illustrated in the lower two panels, which represent an average over 5000 runs. We zoom in to the few e-foldings around horizon crossing to given more details in the left two panels.

In warm inflation, thermal effects decrease until the fluctuations freezes out which is determined by $k^2/a^2 \approx (3H + \gamma)H$, and the freezeout time N_F always precedes the horizon crossing time [40]. According to Fig. 2 we know before freezeout time the system is dominated by stochastic noise, and the initial condition of perturbations have little impact on the final results. In the period between freeze-out and horizon crossing, the power spectrum \mathcal{P}_σ and \mathcal{P}_r may get enhanced due to the coupling between perturbations of radiation and inflaton, as illustrated in the lower left panels of Fig. 2. This growing mode occurs only when $Q_* > 1$ (in the example illustrated in Fig. 2, $Q_* \approx 10$), and in weak regime of warm inflation this is replaced by a constant mode [41]. After horizon-crossing, the power spectrum $\mathcal{P}_\mathcal{R}$ do not change for a while until the turning occurs at background trajectory. When background evolution trajectory change direction, the parameter θ^2 can become large, which will make the the perturbation \mathcal{R}_σ , \mathcal{R}_r coupled strongly with isocurvature perturbation \mathcal{S} as shown in Eqs. (2.18), (2.19) and (2.20). At this moment, \mathcal{R}_σ , \mathcal{R}_r increases obviously while \mathcal{S} decays to zero. In the following period there is only one active scalar field and the curvature perturbation tend to a constant value. We also

know from the top two panels of Fig. 2 that $\mathcal{R}_\sigma \approx \mathcal{R}_r$ on super-horizon scales, and they evolve together until the end of inflation. Therefore, we can use \mathcal{R}_σ to represent curvature perturbation \mathcal{R} according to Eq. (2.12).

IV. CONSTRAINTS FROM OBSERVATIONAL DATA

In previous subsection we have known the main features of background dynamics and perturbation power spectrum in two-field warm inflation, and now we turn to the consistency with observational data. In order to compare with the observational data, we should get the power spectrum $\mathcal{P}_\mathcal{R}$ at the end of inflation first, and then we can obtain the spectral index n_s using finite difference method [42],

$$n_s - 1 = \frac{d \ln \mathcal{P}_\mathcal{R}}{d \ln k}. \quad (4.1)$$

The tensor mode of perturbations is not affected by the thermal noise, so the tensor power spectrum and tensor-

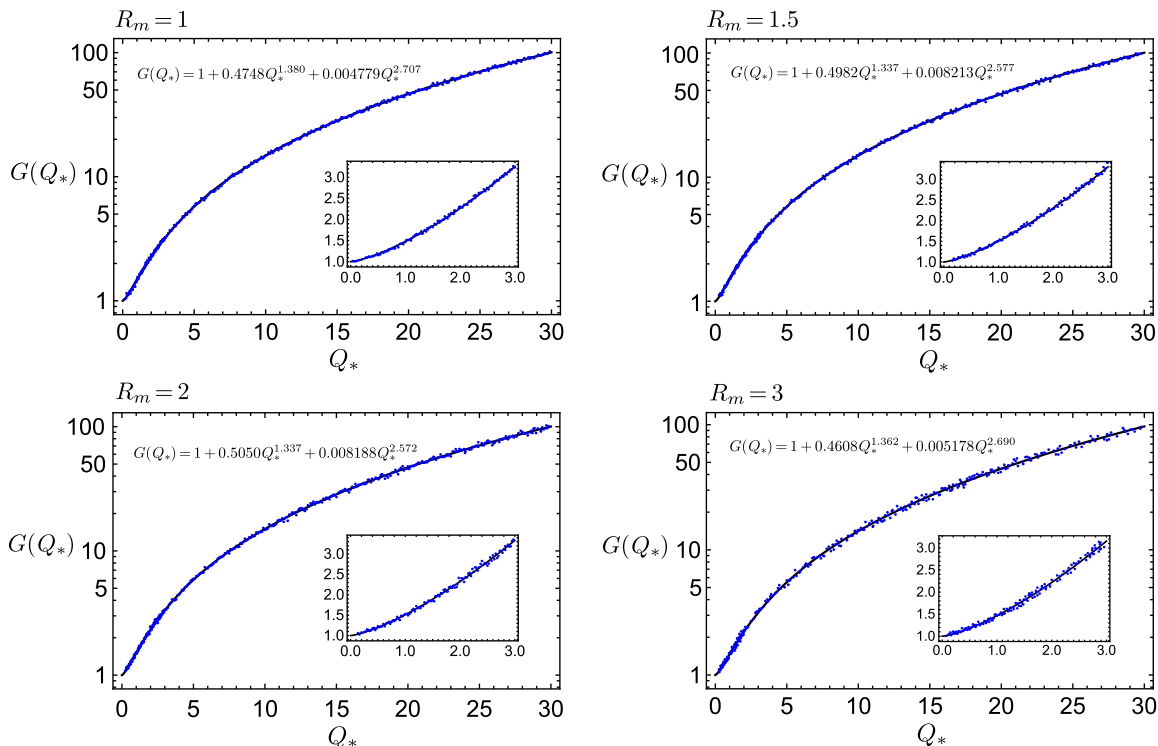


FIG. 3: The numerical results (blue dots) and analytic fitting function of $G(Q_*)$ (black line) are shown against Q_* . In general, the analytic expression $G(Q_*)$ fits well with the numerical results, and the figure shows the growing function $G(Q_*)$ is slightly different for different potentials. At the lower right part of each panel, we zoom in to give more details for small values of Q_* .

to-scalar ratio are given by [43],

$$\mathcal{P}_T = 8 \left(\frac{H_*}{2\pi} \right)^2, \quad r = \frac{\mathcal{P}_T}{\mathcal{P}_\mathcal{R}}. \quad (4.2)$$

There exist two methods available to compute the final $\mathcal{P}_\mathcal{R}$. The most straightforward way is the method we use in the previous section, where we perform our analysis by solving the coupled stochastic system numerically until the end of inflation. However, this is a computationally intensive way and the calculations consumes a long CPU time, because we have to perform tens of thousands of runs to get a relative accurate result. There exists another approach to achieve our purpose which is used more widely. We can use the analytic expression Eq. (2.17) to express $\mathcal{P}_{\delta\sigma}$ at horizon crossing, and the growing function $G(Q_*)$ can be determined by integrating the stochastic

equations a few e-foldings before horizon crossing. After horizon crossing, we can use δN -formalism to get the time evolution of $\mathcal{P}_\mathcal{R}$ until the end of inflation,

$$\mathcal{P}_\mathcal{R} = \mathcal{P}_{\delta\sigma}^* (N_{\phi_*}^2 + N_{\chi_*}^2), \quad (4.3)$$

where $\mathcal{P}_{\delta\sigma}^*$ is the power spectrum of field perturbation $\delta\sigma$ at horizon crossing.

In the following investigation, we take four representative values of mass ratio R_m , $R_m = 1$, $R_m = 1.5$, $R_m = 2$ and $R_m = 3$ as examples. To obtain the growing function $G(Q_*)$ in Eq. (2.17) in two-field warm inflation, we carry out a numerical simulation for each value of R_m . $G(Q_*)$ and numerical results of simulations are shown in Fig. 3. According to Fig. 3, we know the function $G(Q_*)$ fits well with the numerical results.

With a given mass ratio R_m , for every set of initial conditions (ϕ_*, χ_*) , we can determine the value of m_ϕ and C_T using $N_e = 60$ and observational constraints $\mathcal{P}_\mathcal{R} = 2.2 \times 10^{-9}$ at the end of inflation. And then with the value of (m_ϕ, C_T) we can obtain the spectral

index and tensor-to-scalar ratio (n_s, r) with Eqs. (4.1) and (4.2). Therefore, we have a corresponding (n_s, r) for every set of initial condition (ϕ_*, χ_*) . We show the final value of spectral index n_s with initial condition (ϕ_*, χ_*) in Fig. 4. In every panel in Fig. 4, the damping strength

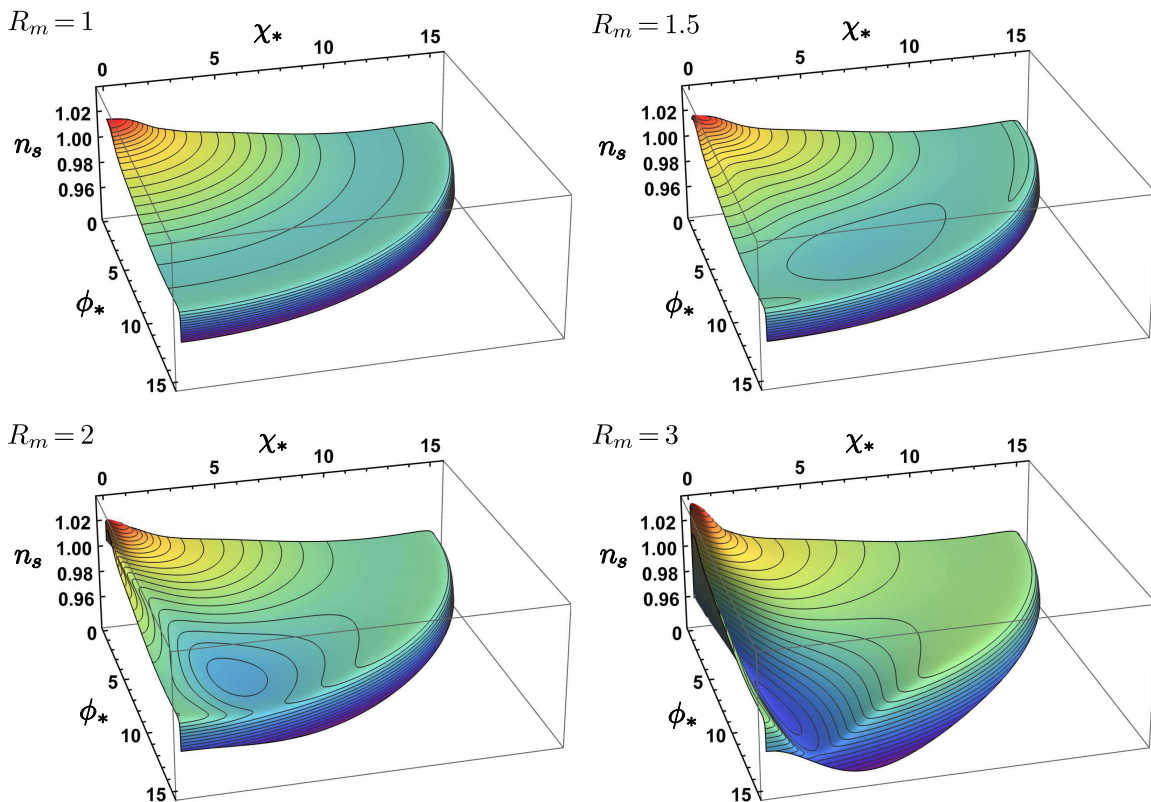


FIG. 4: The final spectral index n_s are plotted against the initial condition (ϕ_*, χ_*) . In each panels, the dissipative ratio Q_* are generally larger when (ϕ_*, χ_*) are closer the the original point $(0, 0)$, and the farthest points in each direction denotes $Q_* = 0$ (cold two-field inflation). The figure also shows that the dissipative effects will render the power spectrum blue-tilted. Meanwhile, multi-field effects will make n_s take values in a wider range.

Q_* is larger when (ϕ_*, χ_*) are near to original point $(0, 0)$. According to the figure we know the strong dissipative effect will render the spectrum blue-tilted, which agree with the conclusion in single-field cases. In all directions, the farthest (ϕ_*, χ_*) from original point represent the case $Q_* = 0$ (cold inflation). We also find when $R_m = 1$ ($m_\phi = m_\chi$), n_s is the same for all the points (ϕ_*, χ_*) of same distance from original point. However,

this property of symmetry no longer exists when $R_m \neq 1$. In fact, when $R_m = 1$, the background evolution trajectory is a straight line in field space of (ϕ, χ) , so there is only one degree of freedom, which is the same as single-field cases. In the following context, we use this case to represent an example of single-field warm inflation for comparison with other cases.

In order to compare our results with observational data directly, we also show our results in (n_s, r) plane, as illustrated in Fig. 5. For each R_m , we plot (n_s, r) in the same plot with the allowed contour plots of Planck data (68% and 95% C.L. results from Planck 2018 TT,TE,EE+lowE+lensing) [44]. Note that in the figure we represent $Q_* = 0$, $Q_* = 1$, and $Q_* = 10$ with thick black lines (the line for $Q_* = 0$ is at the top of the blue-shaded region, which represent the cold inflation cases). As described above, we can treat the $R_m = 1$ case as a single-field warm inflation example. Comparing $R_m = 1$ with other values of R_m , we can conclude that the multi-

field effects will make n_s distribute in a wide range for every value of r , rather than a point. Besides, the dissipative effects have an impact both on the spectral index n_s and tensor-to-scalar ratio r , while the multi-effects have little influence on r . According to Fig. 5 we know in single-field cases, strong version of warm inflation is disfavored by observation for the dissipation will render the spectrum blue-tilted. However, warm inflation can happen when $Q_* > 1$ in multi-field cases. For all cases we studied In Fig. 5, n_s shows oscillatory features when Q_* changes, and this interesting feature also happen in Ref. [37]

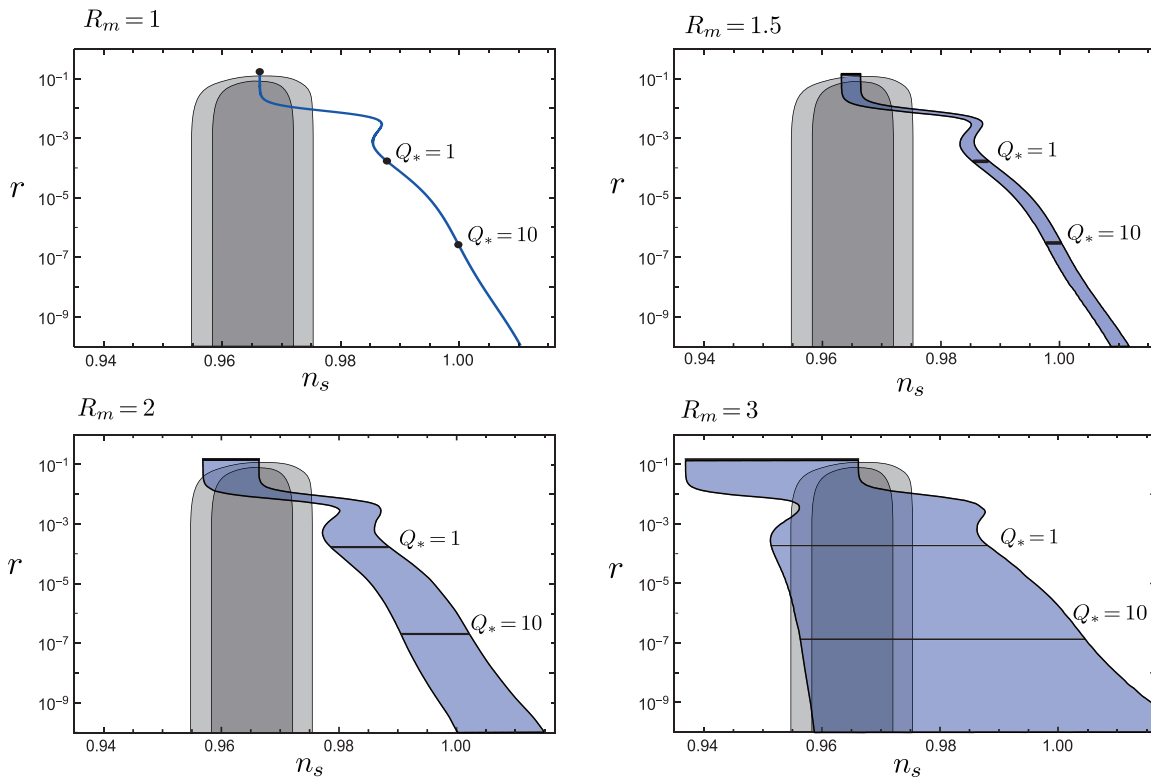


FIG. 5: Observational predictions (blue regions) of two-field warm inflation models with differential mass ratio R_m . The gray contours correspond to the 68% and 95% C.L. results from Planck 2018 TT,TE,EE+lowE+lensing data. Note that when $R_m = 1$, the results are same to the single-field case. The black lines at the top of blue regions in each panel denote $Q_* = 0$ (cold two-field inflation). The lower right panel shows that strong dissipative warm inflation is observationally favored due to the multi-field effects in warm inflation.

We find $Q_* < 0.0018$, $r > 0.0090$ for $R_m = 1$, which means only weak versions of warm inflation is allowed by observation, and this is consistent with the previous studies on single-field warm inflation [45]. When $R_m = 1.5$, the dissipative strength Q_* can take values $Q_* < 0.0024$, and $r > 0.0077$. In case of $R_m = 2$, Q_* lies in

a slight wider range $Q_* < 0.0044$, and r takes values $r > 0.0057$. For $R_m = 3$, Q_* can be as large as 100, which means warm inflation is no longer restricted to weak regimes, and this is very different from single-field cases. In this case, r has a lower bound about 10^{-15} .

Another potential discriminator between different inflationary models is the non-Gaussianity produced during inflation. The nonlinear parameter f_{NL} is given by,

$$f_{\text{NL}} = f_{\text{NL}}^{(3)} + f_{\text{NL}}^{(4)}, \quad (4.4)$$

where $f_{\text{NL}}^{(3)}$ is a slow-roll suppressed term coming from the intrinsic non-Gaussianity in $\delta\phi$ and $\delta\chi$. It has been shown that $f_{\text{NL}}^{(3)}$ is much less than unity [46], which is too small to be observed by the current CMB experiment. Therefore, we will concentrate on the second term $f_{\text{NL}}^{(4)}$,

which can be expressed using δN formalism [15],

$$f_{\text{NL}}^{(4)} = \frac{5}{6} \frac{\sum_{IJ} N_{,IJ} N_{,I} N_{,J}}{\left(\sum_I N_{,I}^2\right)^2}, \quad (4.5)$$

where $N_{,I} = \partial N / (\partial \varphi_*^I)$, $N_{,IJ} = \partial^2 N / (\partial \varphi_*^I \partial \varphi_*^J)$, and the index I, J run over all of the fields.

We have performed some numerical calculations of $f_{\text{NL}}^{(4)}$ using Eq. (4.5), and obtained the final value of $f_{\text{NL}}^{(4)}$ at the end of inflation. According to our results, the nonlinear parameter $f_{\text{NL}}^{(4)} = 2.3 \times 10^{-3}$ for strong dissipative warm inflation, and $f_{\text{NL}}^{(4)} = 6.9 \times 10^{-3}$ for weak dissipative warm inflation. Our results are of the same order of magnitude

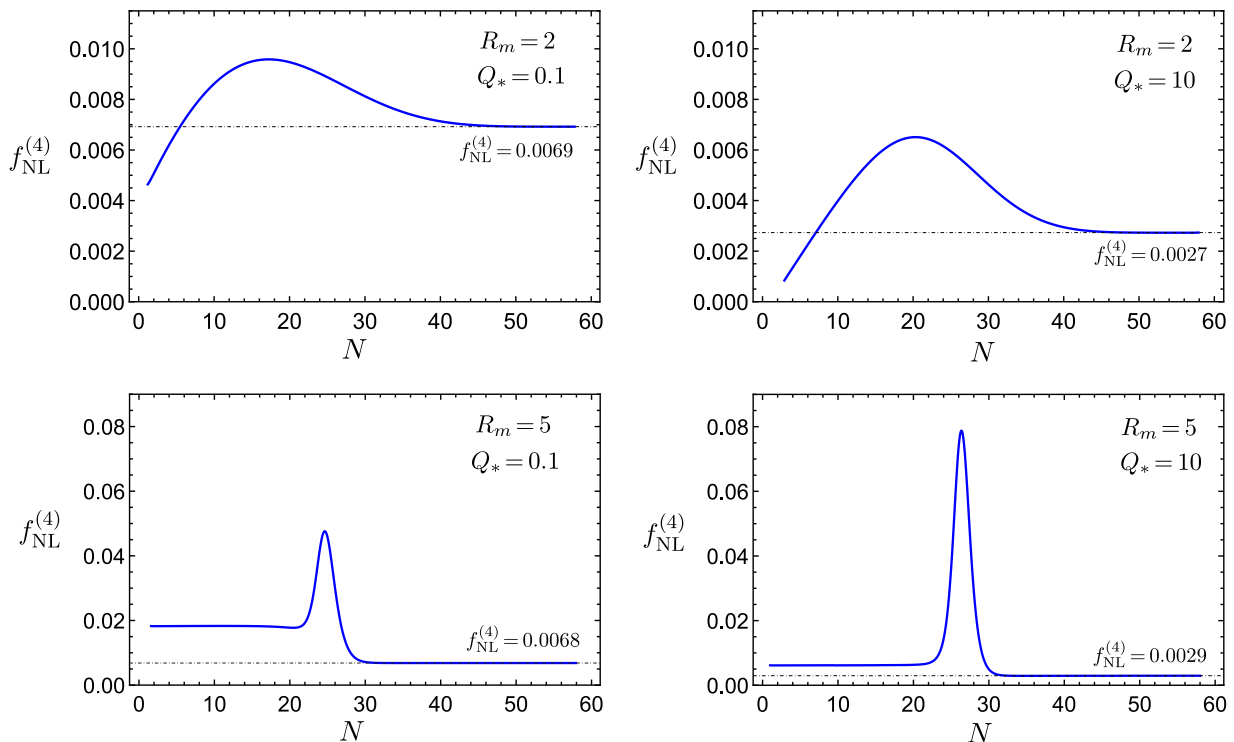


FIG. 6: The evolution of nonlinear parameter $f_{\text{NL}}^{(4)}$. We take $R_m = 2, 5$ and $Q_* = 0.1, 10$, and the values of $f_{\text{NL}}^{(4)}$ at the end of inflation are indicated in each panel. In our numerical examples, turns of trajectories in field space all occur between $N = 10$ and $N = 30$.

as some previous studies on warm inflation and multi-field inflation [13, 20, 47, 48]. In Fig. 6, taking $R_m = 2, 5$ and $Q_* = 0.1, 10$ as examples, we give the evolution of $f_{\text{NL}}^{(4)}$ from Hubble exit until the end of inflation. As illustrated in Fig. 6, $f_{\text{NL}}^{(4)}$ grows sharply when the heavy field decay to zero, corresponding to the turn of trajectory in field space, but then decrease. After this moment,

there is only one effective field and the nonlinear parameter become slow-roll suppressed, which is the same as single-field inflation. We can also conclude from Fig. 6 that multi-field inflation do not necessarily produce large non-Gaussianity, and the mass ratio R_m does not have a significant impact on the final nonlinear parameter $f_{\text{NL}}^{(4)}$.

V. CONCLUSIONS

In this work, we have tried to explore the main features of perturbations in two-field warm inflation, and then use the observational data to constrain our models. We use the two-field quadratic warm inflation model with a linear- T dissipative coefficient as a representative example, and carry out exhaustive numerical simulations to reveal the main features of multi-field warm inflation. Firstly, we derived the full set of equations describing background dynamics and perturbations. Taking into account of the stochastic noise, these are a set of coupled stochastic differential equations (SDE). Then we apply the formula to an example and get the main features of the evolution of perturbations by solving the SDE numer-

ically. We have shown that the curvature perturbation $\mathcal{R} \approx \mathcal{R}_\sigma \approx \mathcal{R}_r$ in super-horizon scales and the isocurvature will decay to zero before the end of inflation. In the following calculation, instead of integrating the SDE to the end of inflation directly, we take a less compute-intensive method to get the power spectrum at the end of inflation. We use an analytic formula Eq. (2.17) to describe $\mathcal{P}_{\mathcal{R}}$ at horizon crossing, in which the growing function $G(Q_*)$ is obtained by fully numerical method. After horizon crossing, δN -formalism is used to get the final power spectrum $\mathcal{P}_{\mathcal{R}}$ at the end of inflation. With the observational constraints $\mathcal{P}_{\mathcal{R}} = 2.2 \times 10^{-9}$ and $N_e = 60$, we obtain a set of (n_s, r) for every initial condition (ϕ_*, χ_*) , as illustrated in Fig. 4. At last, we show our results in (n_s, r) plane in Fig. 5, and compare the observational pre-

dictions of our models with the latest Planck data.

According to Fig. 5, we know that in single-field inflation, warm inflation only occurs in weak dissipative regime, because the strong dissipation will render the power spectrum blue-tilted, which is not compatible with observation. However, the multi-field effects will cause the spectral index n_s take values in a wide range for every r , rather than just a point. In this condition, observations are less effective in constraining n_s , and when the multi-effects is large enough strong versions of warm inflation can become favored by observation.

The thick black line in each panels of Fig. 5 represents $Q_* = 0$ (cold inflation), from which we know the multi-effects will not change the tensor-to-scalar ratio r very much. Therefore, the inflationary models ruled out by observation for predicting to large r may not be rescued in the multi-field case.

The existence of isocurvature perturbations will lead to the time evolution of the curvature perturbation \mathcal{R} , and this evolution can happen even in post-inflationary era. Therefore, multi-field inflation is generally not predictive, unless an adiabatic limit is reached before the end of inflation. Fortunately, in all the cases we studied, the isocurvature mode of perturbations decay to zero before the end of inflation, as illustrated in Fig. 2. However, Fig. 5 shows even in this condition, two-field warm inflation models are not well constrained by the observational results of (n_s, r) , especially when the mass ratio R_m is large. In this case, other observational predictions such as the running of spectral index can be used to constrain inflationary models, and we will leave this to future study. On the other hand, if two mass scales are widely separated, inflation tends to be dominated by only the light field. Under this circumstance, we will go back to single-field warm inflation.

Compared with single-field cases, slow-roll parameters may become relatively large in multi-field warm inflation. We have to go beyond the slow-roll approximations, or some important features will be lost. Fig. 2 shows that the slow-roll parameters ϵ and η have local extremes when the heavy field χ decay to zero, and this effect becomes more obvious when the mass ratio R_m is large. If these extremes occur at horizon crossing by coincidence, the slow-roll corrections will make the analytic expression Eq. (2.17) less accurate in describing the power spectrum at horizon crossing. As demonstrated by Fig. 3, larger R_m will lead to higher residuals when we use the growth function $G(Q_*)$ to fit the data obtained by numerical simulation. A possible way to deal with this problem is that we can integrate the stochastic perturbation equations Eqs. (2.18), (2.19) and (2.20) directly to the end of inflation without introducing the analytic formula Eq. (2.17) at horizon crossing, which is a more compute-extensive method. From this work, we can conclude that even the simplest two-field warm inflation models are much more complicated than single-field cases, and this topic needs further investigations.

Note that in two-field quadratic warm inflation, when

$m_\phi = m_\chi$ the background trajectory in field space is a straight line regardless of the initial conditions. Therefore, the isocurvature mode of perturbation have no influence on curvature perturbation according to Eqs. (2.18), (2.19) and (2.20), so the perturbation features is the same to the single-field case, as illustrated in the top left panel in Fig. 5. However, this property no longer exists in other two-field warm inflation models. For example, in two-field quartic inflation with a potential $V = \frac{1}{4}\lambda_\phi\phi^4 + \frac{1}{4}\lambda_\chi\chi^4$, the $\lambda_\phi = \lambda_\chi$ case is not equivalent to single-field inflation (we describe more details in Appendix B). Besides, the dissipative coefficient γ can be different for ϕ and χ in general. In this work we use a common γ just for simplicity, and this topic needs further study.

VI. ACKNOWLEDGEMENTS

This work was supported by the National Natural Science Foundation of China (Grants No. 11575270, No. 11175019, No. 11235003 and No.11605100).

Appendix A: Perturbation Equations in Multi-field Warm Inflation

In this section, we will present some perturbation equations in multi-field warm inflation. For a multi-component system consisting of two scalar field φ_I ($I = 1, 2$) and a radiation fluid, the Einstein equation of the system is given by [49],

$$G_{\mu\nu} = T_{\mu\nu}^{(\varphi)} + T_{\mu\nu}^{(r)}, \quad (\text{A1})$$

where

$$T_{\mu\nu}^{(\varphi)} = \Sigma_I \partial_\mu \varphi_I \partial_\nu \varphi_I - g_{\mu\nu} \left(\frac{1}{2} \Sigma_I \partial^\lambda \varphi_I \partial_\lambda \varphi_I + V(\varphi) \right), \quad (\text{A2})$$

$$T_{\mu\nu}^{(r)} = (\rho_r + p_r) u_\mu u_\nu + p_r g_{\mu\nu}, \quad (\text{A3})$$

where $G_{\mu\nu}$ is the Einstein tensor, and $T_{\mu\nu}^{(\varphi)}$, $T_{\mu\nu}^{(r)}$ are the energy-momentum tensor of scalar fields and radiation fluid. For the radiation fluid, $p_r = \frac{1}{3}\rho_r$, $\delta p_r = \frac{1}{3}\delta\rho_r$, where p_r , ρ_r are the pressure and energy density of the radiation, and δp_r , $\delta\rho_r$ are their perturbations respectively.

For simplicity, we will work in spatially-flat gauge ($E = \psi = 0$). According to the perturbation equations of Einstein equation, we can represent metric perturbation A , B in terms of perturbations of scalar fields and radiation [50],

$$A = \frac{-\delta q_r + \Sigma_I \dot{\varphi}_I \delta\varphi_I}{2H}, \quad (\text{A4})$$

$$\begin{aligned}
B = & -\frac{a}{4k^2H^2}(24H^2\delta q_r \\
& + (4\rho_r + \Sigma_I\dot{\varphi}_I^2)(-\delta q_r + \Sigma_I\dot{\varphi}_I\delta\varphi_I) \\
& + 2H(3\delta\dot{q}_r + 4\gamma\Sigma_I\dot{\varphi}_I\delta\varphi_I + \Sigma_I\ddot{\varphi}_I\delta\varphi_I - \Sigma_I\dot{\varphi}_I\delta\dot{\varphi}_I)), \quad (A5)
\end{aligned}$$

where $\delta q_r = a(p_r + \rho_r)(B + \delta u)$ is the momentum density perturbation of radiation. The variation of scalar field's equation of motion is given by [51],

$$\begin{aligned}
\delta\ddot{\varphi}_I + (3H + \gamma)\delta\dot{\varphi}_I + \frac{k^2}{a^2}\delta\varphi_I + \Sigma_J V_{\varphi_I\varphi_J}\delta\varphi_J + \dot{\varphi}_I\delta\gamma \\
= -(2V_{\varphi_I} + \gamma\dot{\varphi}_I)A + \dot{\varphi}_I\left(\dot{A} - \frac{k^2}{a}B\right). \quad (A6)
\end{aligned}$$

After some adaption, the perturbation of energy and momentum conservation equations of the radiation leads to [18, 52],

$$\begin{aligned}
\delta\ddot{q}_r + 7H\delta\dot{q}_r + 3\left(7H^2 + \dot{H} + \frac{1}{3}\frac{k^2}{a^2}\right)\delta q_r + \\
\Sigma_I\left(\frac{1}{3}\dot{\varphi}_I^2\delta\gamma + (4H\gamma + \dot{\gamma})\dot{\varphi}_I\delta\varphi_I + \gamma\ddot{\varphi}_I\delta\varphi_I + \frac{5}{3}\gamma\dot{\varphi}_I\delta\dot{\varphi}_I\right) \\
= \frac{1}{3}\frac{k^2}{a}\rho_r B - \frac{16}{3}H\rho_r A + \frac{1}{3}\gamma\Sigma_I\dot{\varphi}_I^2 A - \frac{4}{3}\rho_r\dot{A}. \quad (A7)
\end{aligned}$$

Substituting Eqs. (2.7) and (2.10) into Eqs. (A6) and (A7), we can get,

$$\begin{aligned}
\delta\ddot{\sigma} + (3H + \gamma)\delta\dot{\sigma} + \left(\frac{k^2}{a^2} + V_{\sigma\sigma} - \dot{\theta}^2\right)\delta\sigma - 2\dot{\theta}\delta s \\
+ 2\left(\frac{2\dot{\theta}V_\sigma}{\dot{\sigma}} - \ddot{\theta}\right)\delta s + \dot{\sigma}\delta\gamma \\
= -\frac{k^2}{a}\dot{\sigma}B - (\dot{\sigma}\gamma + 2V_\sigma)A + \dot{\sigma}\dot{A}, \quad (A8)
\end{aligned}$$

$$\begin{aligned}
\delta\ddot{s} + (3H + \gamma)\delta\dot{s} + \left(\frac{k^2}{a^2} + V_{ss} - \dot{\theta}^2\right)\delta s \\
+ 2\dot{\theta}\delta\dot{\sigma} - \frac{2\dot{\theta}\ddot{\sigma}}{\dot{\sigma}}\delta\sigma = 2\dot{\theta}\dot{\sigma}A, \quad (A9)
\end{aligned}$$

$$\begin{aligned}
\delta\ddot{q}_r + 7H\delta\dot{q}_r + 3\left(7H^2 + \dot{H} + \frac{1}{3}\frac{k^2}{a^2}\right)\delta q_r + \\
\frac{5}{3}\gamma\dot{\sigma}\delta\dot{\sigma} + (\gamma\ddot{\sigma} + \dot{\gamma}\dot{\sigma} + 4H\gamma\dot{\sigma})\delta\sigma + \frac{1}{3}\dot{\sigma}^2\delta\gamma - \frac{2}{3}\gamma\dot{\theta}\dot{\sigma}\delta s \\
= \frac{1}{3}\frac{k^2}{a}\rho_r B - \frac{16}{3}H\rho_r A + \frac{1}{3}\gamma\dot{\sigma}^2 A - \frac{4}{3}\rho_r\dot{A}. \quad (A10)
\end{aligned}$$

where

$$V_{\sigma\sigma} = \cos^2\theta V_{\phi\phi} + \sin 2\theta V_{\phi\chi} + \sin^2\theta V_{\chi\chi}, \quad (A11)$$

$$V_{ss} = \sin^2\theta V_{\phi\phi} - \sin 2\theta V_{\phi\chi} + \cos^2\theta V_{\chi\chi}. \quad (A12)$$

Substituting Eqs. (A4), (A5) into Eqs. (A8), (A9), (A10), and express the equations in terms of \mathcal{R}_σ , \mathcal{R}_r using $\mathcal{R}_\sigma = H\delta\sigma/\dot{\sigma}$, $\mathcal{R}_r = -H\delta q_r/(p_r + \rho_r)$, we get

$$\begin{aligned}
\ddot{\mathcal{R}}_\sigma + \left(3H + \gamma + \frac{4\rho_r}{3H} + \frac{\dot{\sigma}^2}{H} + \frac{2\ddot{\sigma}}{\dot{\sigma}}\right)\dot{\mathcal{R}}_\sigma + \left(\frac{k^2}{a^2} + H\gamma - \dot{\theta}^2 + \frac{4\rho_r}{3} + \frac{2\gamma\rho_r}{3H} + \frac{8\rho_r^2}{9H^2} - \frac{11\gamma\dot{\sigma}^2}{6H} - \frac{\gamma^2\dot{\sigma}^2}{\rho_r} + \frac{4\rho_r\ddot{\sigma}}{3H\dot{\sigma}}\right)\mathcal{R}_\sigma \\
= -\left(\gamma + \frac{4\rho_r}{3H}\right)\dot{\mathcal{R}}_r + \left(H\gamma + \frac{4\rho_r}{3} + \frac{2\gamma\rho_r}{3H} + \frac{8\rho_r^2}{9H^2} - \frac{11\gamma\dot{\sigma}^2}{6H} - \frac{\gamma^2\dot{\sigma}^2}{\rho_r} + \frac{4\rho_r\ddot{\sigma}}{3H\dot{\sigma}}\right)\mathcal{R}_r \\
+ \frac{2H\dot{\theta}}{\dot{\sigma}}\delta\dot{s} + \left(\frac{6H^2\dot{\theta}}{\dot{\sigma}} + \frac{2H\gamma\dot{\theta}}{\dot{\sigma}} + \frac{2H\ddot{\theta}}{\dot{\sigma}} + \dot{\theta}\dot{\sigma} + \frac{2H\dot{\theta}\ddot{\sigma}}{\dot{\sigma}^2}\right)\delta s, \quad (A13)
\end{aligned}$$

$$\begin{aligned}
\ddot{\mathcal{R}}_r + \left(-H + \frac{4\rho_r}{3H} + \frac{\dot{\sigma}^2}{H} + \frac{7\gamma\dot{\sigma}^2}{4\rho_r}\right)\dot{\mathcal{R}}_r + \left(\frac{k^2}{3a^2} + \frac{3\gamma\dot{\sigma}^2}{2H} + \frac{9H\gamma\dot{\sigma}^2}{4\rho_r} + \frac{8\rho_r\dot{\sigma}^2}{9H^2} + \frac{\dot{\sigma}^4}{2H^2} + \frac{7\gamma\dot{\sigma}^4}{8H\rho_r} + \frac{\dot{\sigma}\ddot{\sigma}}{H} + \frac{2\gamma\dot{\sigma}\ddot{\sigma}}{\rho_r}\right)\mathcal{R}_r \\
= \left(\frac{\dot{\sigma}^2}{3H} + \frac{5\gamma\dot{\sigma}^2}{4\rho_r}\right)\dot{\mathcal{R}}_\sigma + \left(\frac{3\gamma\dot{\sigma}^2}{2H} + \frac{9H\gamma\dot{\sigma}^2}{4\rho_r} + \frac{8\rho_r\dot{\sigma}^2}{9H^2} + \frac{\dot{\sigma}^4}{2H^2} + \frac{7\gamma\dot{\sigma}^4}{8H\rho_r} + \frac{\dot{\sigma}\ddot{\sigma}}{H} + \frac{2\gamma\dot{\sigma}\ddot{\sigma}}{\rho_r}\right)\mathcal{R}_\sigma \\
+ \left(-\frac{1}{3}\dot{\theta}\dot{\sigma} + \frac{H\gamma\dot{\theta}\dot{\sigma}}{2\rho_r}\right)\delta s, \quad (A14)
\end{aligned}$$

$$\ddot{\delta s} + (3H + \gamma)\dot{\delta s} + \left(\frac{k^2}{a^2} - \dot{\theta}^2 + V_{ss}\right)\delta s = -\frac{2\dot{\theta}\dot{\sigma}}{H}\mathcal{R}_\sigma - \frac{4\dot{\theta}\dot{\sigma}\rho_r}{3H^2}\mathcal{R}_\sigma + \frac{4\dot{\theta}\dot{\sigma}\rho_r}{3H^2}\mathcal{R}_r. \quad (\text{A15})$$

Note that in case of $\gamma = C_T T$, we have $\delta\gamma/\gamma = \delta T/T = \delta\rho_r/(4\rho_r)$, and $\delta\gamma$ has been eliminated from perturbation equations. Taking into account of the stochastic noise ξ and change the time variable from cosmic time t to e-foldings N , we can obtain the perturbation equations in Section II.

Appendix B: Two-field quadratic inflation with equal masses

According to background equations Eqs. (2.22) and (2.23), in case of $m_\phi = m_\chi = m$, for two-field quadratic inflation we have,

$$\phi'' + (3 + 3Q - \epsilon)\phi' + m^2\phi/H^2 = 0, \quad (\text{B1})$$

$$\chi'' + (3 + 3Q - \epsilon)\chi' + m^2\chi/H^2 = 0, \quad (\text{B2})$$

After some adaption, the above equations can be put in the form,

$$(\phi'\chi - \chi'\phi)' + (3 + 3Q - \epsilon)(\phi'\chi - \chi'\phi) = 0. \quad (\text{B3})$$

The solution of the above equation is given by,

$$(\phi'\chi - \chi'\phi) = C e^{-\int_0^N (3+3Q-\epsilon)dN}, \quad (\text{B4})$$

where C is an integration constant. During inflation, $Q > 0$ and $\epsilon < 1$, therefore,

$$|\phi'\chi - \chi'\phi| < |C| e^{-\int_0^N 2dN} = |C| e^{-2N}. \quad (\text{B5})$$

From Eq. (B5), we know $\phi'\chi - \chi'\phi$ will tend to zero rapidly. When $(\phi/\chi)' = (\phi'\chi - \chi'\phi)/\chi^2 \sim 0$, the trajectory in field space will become a straight line, which is the same as the single-field case.

However, for two-field quartic inflation $V = \frac{1}{4}\lambda_\phi\phi^4 + \frac{1}{4}\lambda_\chi\chi^4$, the effective mass $m_\phi = V_{\phi\phi}$ and $m_\chi = V_{\chi\chi}$ are not constants during inflation, and in general Eq. (B3) is not valid even for $\lambda_\phi = \lambda_\chi$. In this case, we cannot reach the above conclusion, and the background dynamics of two-field quartic inflation display more complex behavior.

-
- [1] A. H. Guth, ‘‘Inflationary universe: a possible solution to the horizon and flatness’’, *Phys. Rev. D* 23, 347 (1981).
 - [2] A. D. Linde, ‘‘A new inflationary universe scenario: a possible solution of the horizon, flatness, homogeneity, isotropy and primordial monopole problems’’, *Phys. Lett. B* 108, 389 (1982).
 - [3] J. Yokoyama and K. Maeda, ‘‘On the dynamics of the power law inflation due to an exponential potential’’, *Phys. Lett. B* 207, 31 (1988).
 - [4] A. Berera, I. G. Moss and R. O. Ramos, ‘‘Warm inflation and its microphysical basis’’, *Rept. Prog. Phys.* 72, 026901 (2009). arXiv:0808.1855 [hep-ph].
 - [5] X. B. Li, Y. Y. Wang, H. W and J. Y. Zhu, ‘‘Dynamic analysis of noncanonical warm inflation’’, *Phys. Rev. D* 98, 043510 (2018).
 - [6] M. Bastero-Gil, A. Berera, R. O. Ramos and J. G. Rosa, ‘‘Adiabatic out-of-equilibrium solutions to the boltzmann equation in warm inflation’’, *JHEP* 02 (2018) 063.
 - [7] X. M. Zhang, J. Y. Zhu, ‘‘Consistency of the tachyon warm inflationary universe models’’, *JCAP* 02 (2014) 005.
 - [8] A. Berera, J. Mabillard, M. Pieroni and R. O. Ramos, ‘‘Identifying universality in warm inflation’’, *JCAP* 07 (2018) 021.
 - [9] J. Yokoyama and A. Linde, ‘‘Is warm inflation possible?’’, *Phys. Rev. D* 60, 083509 (1999). arXiv:9809409 [hep-ph].
 - [10] M. Bastero-Gil, A. Berera, R. O. Ramos and J. G. Rosa, ‘‘Warm little inflaton’’, *Phys. Rev. Lett.* 117, 151301 (2016). arXiv:1604.08838 [hep-ph].
 - [11] Z. Lalak, D. Langlois, S. Pokorski and K. Turzynski, ‘‘Curvature and isocurvature perturbations in two-field inflation’’, *JCAP* 07 (2007) 014. arXiv:0704.0212 [hep-th].
 - [12] S. Weinberg, *Cosmology*. Oxford University Press, 2008.
 - [13] F. Vernizzi and D. Wands, ‘‘Non-Gaussianities in two-field inflation’’, *JCAP* 05 (2006) 019. arXiv:0603799 [astro-ph].
 - [14] X. M. Zhang and J. Y. Zhu, ‘‘Primordial non-Gaussianity in noncanonical warm inflation’’, *Phys. Rev. D* 91, 063510 (2015).
 - [15] R. de Putter, J. Gleyzes and O. Doré, ‘‘The next non-Gaussianity frontier: what can a measurement with $\sigma(f_{\text{NL}}) \lesssim 1$ tell us about multifield inflation?’’, *Phys. Rev. D* 95, 123507 (2016).
 - [16] I. Huston, ‘‘The evolution of non-adiabatic pressure perturbations during multi-field Inflation’’, *Phys. Rev. D* 85, 063507 (2012).
 - [17] S. Renaux-Petela and K. Turzyński, ‘‘On reaching the adiabatic limit in multi-field inflation’’, *JCAP* 06 (2015) 010.
 - [18] Y. Y. Wang, J. Y. Zhu and X. M. Zhang, ‘‘Two-field Warm Inflation and Its Scalar Perturbations on Large Scales’’, *Phys. Rev. D* 97, 063510 (2018).
 - [19] C. Gordon, D. Wands, B. A. Bassett and R. Maartens, ‘‘Adiabatic and entropy perturbations on inflation’’, *Phys. Rev. D* 63, 023506 (2001). arXiv:0009131 [astro-ph].
 - [20] K. Y. Choi, L. M. H. Hall and C. van de Bruck, ‘‘Spectral running and non-Gaussianity from slow-roll inflation in generalized two-field models’’, *JCAP* 02 (2007) 029.

- arXiv:0701247 [astro-ph].
- [21] S. Tsujikawa, D. Parkinson and B. A. Bassett, “Correlation-consistency cartography of the double-inflation landscape”, *Phys. Rev. D* 67, 083516 (2003).
- [22] R. Kabir and A. Mukherjee, “Oscillatory power spectrum and strongly k -dependent r in hybrid inflation”. arXiv:1602.01221 [gr-qc].
- [23] K. A. Malik and D. Wands, “Adiabatic and entropy perturbations with interacting fluids and fields”, *JCAP* 02 (2005) 007, arXiv:0411703 [astro-ph].
- [24] K. A. Malik, “Cosmological perturbations in an inflationary universe”. arXiv:0101563 [astro-ph].
- [25] S. Cespedes, V. Atal, and G. A. Palma, “On the importance of heavy fields during inflation”, *JCAP* 05 (2012) 008.
- [26] I. G. Moss and C. Xiong, “Non-Gaussianity in fluctuations from warm inflation”, *JCAP* 04 (2007) 007. arXiv:0701302 [astro-ph].
- [27] L. M. H. Hall and I. G. Moss, “Scalar perturbation spectra from warm inflation”, *Phys. Rev. D* 69, 083525 (2004).
- [28] W. L. Lee and L. Z. Fang, “A relativistic calculation of super-Hubble suppression of inflation with thermal dissipation”, *Class. Quant. Grav.*, 17, 4467 (2000).
- [29] C. Graham and I. G. Moss, “Density fluctuations from warm inflation”, *JCAP* 07 (2009) 013.
- [30] N. Videla, “Observational constraints on warm quasi-exponential inflation”, *Phys. Rev. D* 97, 123503 (2018).
- [31] L. Visinelli, “Observational constraints on monomial warm inflation”, *JCAP* 07 (2016) 054.
- [32] M. Bastero-Gil, A. Berera, and R. O. Ramos, “Shear viscous effects on the primordial power spectrum from warm inflation”, *JCAP* 07 (2011) 030.
- [33] A. R. Liddle and D. H. Lyth, *Cosmological Inflation and Large-Scale Structure*. Cambridge University Press, 2000.
- [34] R. O. Ramos and L. A. da Silva, “Power spectrum for inflation models with quantum and thermal noises”, *JCAP* 03 (2013) 032.
- [35] T. Matsuda, “Evolution of the curvature perturbations during warm inflation”, *JCAP* 06 (2009) 002. arXiv:0905.0308 [astro-ph.CO].
- [36] M. Bastero-Gil, A. Berera and N. Kronberg, “Exploring the parameter space of warm-inflation models”, *JCAP* 12 (2015) 046.
- [37] M. Bastero-Gil, S. Bhattacharya, K. Dutta and M. R. Gangopadhyay, “Constraining warm inflation with CMB data”, *JCAP* 02 (2018) 054.
- [38] M. Bastero-Gil, A. Berera, R. Hernández-Jiménez and J. G. Rosa, “Dynamical and observational constraints on the warm little inflaton scenario”, *Phys. Rev. D* 98, 083502 (2018).
- [39] B. Feng and X. Zhang, “Double inflation and the low CMB quadrupole”, *Phys. Lett. B* 570, 145 (2003).
- [40] K. Li, X. M. Zhang, H. Y. Ma and J. Y. Zhu, “Noncanonical warm inflation: A model with a general Lagrangian density”, *Phys. Rev. D* 98, 123528 (2018).
- [41] M. Bastero-Gil, A. Berera, I. G. Moss and R. O. Ramos, “Cosmological fluctuations of a random field and radiation fluid”, *JCAP* 05 (2014) 004.
- [42] M. Dias, J. Frazer and D. Seery, “Computing observables in curved multifield models of inflation—A guide (with code) to the transport method”, *JCAP* 12 (2015) 030. arXiv:1502.03125 [astro-ph.CO].
- [43] A. Riotto, “Inflation and the theory of cosmological perturbations”. arXiv:0210162 [hep-ph].
- [44] Planck Collaboration: Y. Akrami, et al., “Planck 2018 results. X. Constraints on inflation”. arXiv:1807.06211 [astro-ph.CO].
- [45] M. Benetti and R. O. Ramos, “Warm inflation dissipative effects: Predictions and constraints from the Planck data”, *Phys. Rev. D* 95, 023517 (2017).
- [46] D. H. Lyth and I. Zaballa, “Non-Gaussianity of the primordial perturbation in the curvaton model”, *JCAP* 10 (2005) 005. arXiv:0507608 [astro-ph].
- [47] S. Gupta, “Dynamics and non-Gaussianity in the weak-dissipative warm inflation scenario”, *Phys. Rev. D* 73, 083514 (2006).
- [48] D. Battefeld and T. Battefeld, “Non-Gaussianities in N -flation”, *JCAP* 05 (2007) 012. arXiv:0703012 [hep-th].
- [49] Z. P. Peng, J. N. Yu, X. M. Zhang and J. Y. Zhu, “Perturbation spectra in the warm k -inflation”, *Phys. Rev. D* 97, 063523 (2018).
- [50] N. Bartolo, P. Corasaniti, A. Liddle, and M. Malquarti, “Perturbations in cosmologies with a scalar field and a perfect fluid”, *Phys. Rev. D* 70, 043532 (2004). arXiv:0311503 [astro-ph].
- [51] I. Huston and A. J. Christopherson, “Isocurvature perturbations and reheating in multi-field inflation”, arXiv:1302.4298 [astro-ph.CO].
- [52] C. Pitrou, X. Roy and O. Umeh, “xPand: An algorithm for perturbing homogeneous cosmologies”, *Class. Quant. Grav.* 30, 165002 (2013). arXiv:1302.6174 [astro-ph.CO].